CAVITATING FLOW SIMULATIONS BASED ON THE BUBBLE DYNAMICS

Yoshiaki Tamura, Kazuyasu Sugiyama and Yoichiro Matsumoto
University of Tokyo, bunkyoku, Tokyo, Japan

Abstract
A new numerical method for simulating cavitating flows is developed. The cavitation is modeled with the dynamics of bubbles which radii change with Rayleigh-Plesset equation. The pressure inside of a bubble is modeled from the results of very precise direct simulation of single bubble motion. The bubbles are also allowed to have slip velocities so that the bubble accumulation could be simulated. Pseudocompressibility concept for incompressible flow simulation is extended for the present systems of equations for efficient and robust computations. Computations of two- and three-dimensional cavitating flows verify the present method and show its capability to the practical applications of cavitating flows.

1 Introduction
Computational Fluid Dynamics (CFD) has made progress in the last two decades and now it is applied to a variety of practical flow fields, such as a flow around a complete aircraft, a flow in a compressor or a turbine, and so on. However, there is still a large application area that the current CFD technology is not sufficiently applied to. One of them is cavitating flow. There might be two reasons that make the simulation of cavitating flows difficult. One is that the flow is multi-phase. Gas and liquid phases coexist and show more complex nature than either single phase. Also phase change may occur due to the pressure change. The other reason, which is more critical for numerical approaches utilizing temporal and spatial discretization, is scale problem. Cavitation bubbles are much smaller and rapidly act than the global flow structure. It is almost impossible to solve both scales together and we need some model for cavitation or cavitation bubbles inevitably. In the literature, there are papers and articles claiming the cavitating flow simulation (Chen and Heister 1996, Delaunay and Kueny 1990, Lemonnier and Row 1988, kubota et al. 1992, Merkle et al. 1998, Kunz et al. 1999). As seen in the references, however, many of them do use rather empirical cavitation models (pressure-density-void fraction relation, for instance) than physical modeling of cavitation or cavitation bubbles. Most of their approach lack nonequilibrium nature of bubble motion. Even so, the scale problems make their simulations stiff (hard to solve, or easy to blow up) and time consuming. One of the present authors has developed a simplified model of motion of a single cavitation bubbles based on the precise analysis of it. In the present paper, the numerical simulation method of cavitating flow with the simplified bubble dynamics model is described. As the governing equations are very stiff, pseudocompressibility is introduced to relieve the stiffness and loosen the restriction of time step. In the next section, the present method is described in detail. Both two- and three-dimensional flows are simulated to show efficiency and capability of the present method. In the following section, the results are compared with experiments and discussed.

(a) VOF method image. (b) Present model image.

Figure 1: Schematic pictures of cavitation models.

2 Numerical method
2.1 Basic idea
Many existing cavitation models in the literature are categorized in VOF (volume of fraction) method or two-fluid model which is schematically shown in Fig. 1 (a). This works for sheet cavitations or very large (compared with the

computational grid size) bubbles. On the other hand, we star from a single cavitation bubble because the dynamics of cavitation bubble, which is normally smaller than the grid cell size, has influence on the global flow structures. From this observation, cavitation is modeled with groups of many small and locally uniform cavitation bubbles as shown in Fig. 1 (b). Mass and momentum conservations of the fluid are solved with spatially averaged equations as well as the motions of cavitation bubbles. In the following subsections, assumptions will be proposed to derive the governing equations of the image of Fig. 1 (b).

2.2 Assumptions

Followings are assumed to construct the governing equations.

- Liquid phase is incompressible, gas phase is compressible.
- Density and momentum of gas phase is sufficiently small compared to liquid phase.
- Gas phase consists of bubbles, all bubbles are spherical and no collision and coalescence occurs.
- Mass change due to the phase change is much smaller than the mass of liquid.
- Bubbles are filled with vapor and non-condensable gas. The pressure inside a bubble is uniform. The vapor pressure is constant. The pressure of non-condensable gas is modeled to simulate the motion of the bubble observed in very precise computation (Takemura and Matsumoto 1994).

As we start from a single bubble motion, the gas phase is assumed to consist of groups of bubbles. As no collision and coalescence is allowed, high void fraction cannot be treated or, even possible, the solution around such area is not reliable. Also it is implicitly assumed that the bubbles are small enough compared with the grid cell and can be considered locally uniform in one grid cell. Other assumptions are physical and sufficiently reliable solutions are expected for the cavitating flow simulations.

2.3 Governing equations

According the assumptions, the following equations are derived. The dependent variables are number density, radius and velocity of bubbles and pressure and velocity of liquid phase. Note that each bubble is not traced in Lagrangean form but the number density and radius distributions are calculated in Eulerian form as described later.

1) Conservation of the number density of bubbles

$$\frac{\partial n_G}{\partial t} + J\frac{\partial\left(n_G U_{Gi}/J\right)}{\partial \xi_i} = 0. \tag{1}$$

2) Translational motion of a bubble

$$F_{Ii} + F_{Ai} + F_{Pi} + F_{Di} + F_{Li} + F_{Hi} = 0. \tag{2}$$

Here F_{Ii} is the inertia force of a bubble and F_{Hi} is a history force and both are neglected. F_{Ai} is an added mass force and denotes,

$$F_{Ai} = \frac{4}{3}\pi\beta\left(\frac{\partial\left(r_G^3\rho_L u_{Gi}\right)}{\partial t} + U_{Gj}\frac{\partial\left(r_G^3\rho_L u_{Gi}\right)}{\partial \xi_j} - \frac{\partial\left(r_G^3\rho_L u_{Li}\right)}{\partial t} + U_{Lj}\frac{\partial\left(r_G^3\rho_L u_{Li}\right)}{\partial \xi_j}\right), \tag{3}$$

β is taken as 1/2 for a spherical bubble. The subscript L denotes the liquid phase, G the gas phase, i the x, y, z direction, j the ξ,η,ζ direction in the computational domain. U is the contravariant velocity. F_{Pi} is the force by the acceleration of surrounding fluid and,

$$F_{Pi} = -\frac{4}{3}\pi r_G^3\rho_L\left(\frac{\partial u_{Li}}{\partial t} + U_{Lj}\frac{\partial u_{Li}}{\partial \xi_j}\right). \tag{4}$$

Drag and lift forces are given as,

$$\begin{aligned} F_{Di} &= \frac{1}{2}\pi r_G^2\rho_L C_D\left|\vec{u}_G - \vec{u}_L\right|\left(u_{Gi} - u_{Li}\right), \\ F_{Li} &= \frac{1}{2}\pi r_G^2\rho_L C_L\left|\vec{u}_G - \vec{u}_L\right|\varepsilon_{ijk}\omega_{Lk}\left(u_{Gj} - u_{Lj}\right)/\left|\vec{\omega}_L\right|, \end{aligned} \tag{5}$$

$\vec{\omega}_L$ is vorticity vector and their coefficients are,

$$C_D = \frac{24}{Re_{bub}}\left(1 + 0.15 Re_{bub}^{0.687}\right),\ Re_{bub} = \frac{2 r_G \rho_L |\vec{u}_G - \vec{u}_L|}{\mu_L},\ C_L = 0.59 \left(\frac{|\vec{\omega}_L| r_G}{|\vec{u}_G - \vec{u}_L|}\right)^{0.25}. \quad (6)$$

3) volumetric motion of a bubble (Rayleigh-Plesset Equations)

$$r_G \frac{D^2 r_G}{Dt^2} + \frac{3}{2}\left(\frac{Dr_G}{Dt}\right)^2 = \frac{p_B - p_L}{\rho_L} + \frac{1}{4}\left(u_{Li} - u_{Gi}\right)\left(u_{Li} - u_{Gi}\right), \quad (7)$$

p_B is a pressure inside of a bubble and given as,

$$p_B = p_v + p_G - \frac{2T}{r_G} - 4\mu \frac{1}{r_G}\frac{Dr_G}{Dt}. \quad (8)$$

T is the surface tension and p_v is the vapor pressure and both are constant. p_G is the pressure of non-condensable gas and modeled to simulated the single bubble motion as,

$$p_G r_G^3 = const.\ (Dr_G/Dt > 0), \quad p_G r_G^{3\kappa} = const.\ (Dr_G/Dt < 0), \quad (9)$$

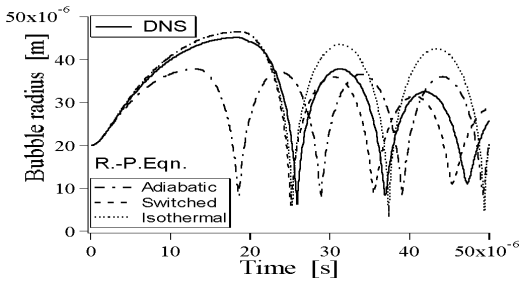

Figure 2: Bubble dynamics model.

κ is the specific heat ratio and taken to be 1.4. This is the simplified model from the observation of a very precise simulation (Takemura and Matsumoto 1994) that the cavitation bubble behaves as if isothermally when expanding and as if adiabatically when shrinking after the complex interface phenomena. The validation of this model is shown in Fig. 2. The line labeled "DNS" is a result of the precise simulation. Others in Fig. 2 are results of the Rayleigh-Plesset equation with different models of non-condensable gas. The line labeled "Switched" corresponds to the present model and follows the DNS line well.

4) Conservation of the volumetric fraction of liquid phase

$$\frac{\partial f_L}{\partial t} + J\frac{\partial\left(f_L U_{Lj}/J\right)}{\partial \xi_j} = 0. \quad (10)$$

This is lead from the mass conservation of mixture with the assumption that the liquid is incompressible and the density of the gas is neglected.

5) Conservation of momentum

$$\frac{\partial\left(\rho_L f_L u_{Li}\right)}{\partial t} + J\frac{\partial\left(\rho_L f_L u_{Li} U_{Lj}/J\right)}{\partial \xi_j} = -\ {}_i p + \ {}_j\left(\mu\ {}_j u_{Li}\right) + \frac{1}{3}\ {}_i\left(\mu\ {}_k u_{Lk}\right). \quad (11)$$

Here the density of gas is neglected. f_L is the volumetric fraction of liquid phase. μ is effective viscosity of bubbly flow and given as,

$$\mu = \left\{1 + f_G\left(\frac{\mu_L + 5/2\,\mu_G}{\mu_L + \mu_G}\right)\right\}\mu_L \quad \left\{1 + f_G\right\}\mu_L, \quad (12)$$

f_G is the void fraction.

6) Constraint of volumetric fractions

$$f_G + f_L = 1 = \frac{4}{3}\pi r_G^3 n_G + f_L. \quad (13)$$

This closes the system of equations.

2.4 Introduction of pseudocompressibility

Above equations do not give pressure directly, just as the same as single phase incompressible flows. Besides f_L and f_G are obtained individually and the constraint (13) thus requires an iterative procedure. Matsumoto et al. (1998) solved this system of equations by HSMAC-like iterative method and resulted in large amount of computation time and did not maintain stability in some cases.

In the present research, pressure is taken as the unknown variable from Eq. (10) for f_L with the idea of pseudocompressibility and f_L is obtained from f_G through Eq. (13).
With the constraint of the volumetric fractions, the density change of the liquid phase is formally described as,

$$\frac{\partial\left(f_G + f_L - 1\right)\rho_L}{\partial t} = \rho_L\left(\frac{\partial f_G}{\partial t} + \frac{\partial f_L}{\partial t}\right) - \frac{\partial \rho_L}{\partial t} = 0 . \tag{14}$$

The time derivative of the density is replaced with $\partial\rho_L / \partial t = 1/ c^2 \;\partial p / \partial t$ as the same as the pseudocompressibility method. c^2 is a coefficient. Substituting Eqs. (1), (10) and $f_G = 4/3\pi r_G^3 n_G$, finally one obtains,

$$\frac{1}{c^2}\frac{\partial p}{\partial t} + \;\;{}_j f_L u_{Lj} + \;\;{}_j f_G u_{Gj} - 4\pi r_G^2 n_G \frac{Dr_G}{Dt} = 0 . \tag{15}$$

Equation (15) is solved instead of Eq. (10) which is automatically satisfied when the pressure goes to steady state.

2.5 Numerical Algorithm

The outline of the numerical procedure is a) solving Eqs. (1), (11) and (15) for the number density of the bubbles, the momentum of the liquid and the pressure; b) solving Eq. (7) for the radii of the bubbles and obtaining the liquid fraction from Eq. (13); c) solving Eq. (2) for the velocity of the bubbles.
Equations (1), (11) and (15) are written in a vector form on generalized coordinates as,

$$\frac{\partial \hat{Q}}{\partial t} + \frac{\partial \hat{E}}{\partial \xi} + \frac{\partial \hat{F}}{\partial \eta} + \frac{\partial \hat{G}}{\partial \zeta} = \frac{\partial \hat{E}_v}{\partial \xi} + \frac{\partial \hat{F}_v}{\partial \eta} + \frac{\partial \hat{G}_v}{\partial \zeta} + \hat{H} \tag{16}$$

where,

$$\hat{Q} = \begin{bmatrix} n_G \\ f_L u_L \\ f_L v_L \\ f_L w_L \\ p \end{bmatrix} / J, \; \hat{E} = \begin{bmatrix} n_G U_G \\ f_L u_L U_L + \xi_x p \\ f_L v_L U_L + \xi_y p \\ f_L w_L U_L + \xi_z p \\ f_L U_L + f_G U_G \end{bmatrix} / J \tag{17}$$

and so on. As the left hand side of Eq. (16) is hyperbolic, a solution method for compressible flows is applied. The convective terms are discretized with so-called flux difference splitting as,

$$\frac{\partial E}{\partial \xi} \quad \frac{\hat{E}_{j+1/2} - \hat{E}_{j-1/2}}{\Delta\xi}, \quad \hat{E}_{j+1/2} = \frac{1}{2}\left[\hat{E}_R + \hat{E}_L - \left|\frac{\partial \hat{E}}{\partial \hat{Q}}\right|_{ave}\left(\hat{Q}_R - \hat{Q}_L\right)\right] \tag{18}$$

where L, R denotes he values of either side of the cell interfaces. In the present case, however, the diagonalization of the flux Jacobian $\partial \hat{E} / \partial \hat{Q}_{ave}$ is difficult because of the complexity of the system. The simplest approximation of the flux Jacobian is to replace all Eigenvalues with the spectral radius as,

$$\hat{E}_{j+1/2} = \frac{1}{2}\left[\hat{E}_R + \hat{E}_L - \sigma_{max}\;\mathbf{I}\left(\hat{Q}_R - \hat{Q}_L\right)\right] \tag{19}$$

Eigenvalues of the present flux Jacobian are also difficult to obtain but under the assumption that the slip velocity $\left(\vec{u}_L - \vec{u}_G\right)$ is zero, the approximated eigenvalues are obtained as, $\left(U_L, U_L, U_L, U_L \pm \sqrt{U_L^2 + c^2\left(\xi_x^2 + \xi_y^2 + \xi_z^2\right)/\; f_L}\right)$ and $\sigma_{max} = \left|U_L\right| + \sqrt{U_L^2 + c^2\left(\xi_x^2 + \xi_y^2 + \xi_z^2\right)/ f_L}$. This scheme is called Lax-Friedrich's and works well for inviscid flow simulations. However, for viscous flow simulations, this scheme introduces large amount of artificial viscosity in boundary layers and a matrix-type (but again approximated) artificial viscosity is also used in some cases. Finally, MUSCL interpolation (van Leer 1979) is used to obtain L, R values of higher-order accuracy.
The viscous terms are discretized with the second order central differences. LU-SGS (Yoon and Jameson 1988) is used for the time integration. Equation (2), which is also a hyperbolic equation for the slip velocity, is discretized with MUSCL interpolation and again integrated by LU-SGS. Equation (7) of Rayleigh-Plesset is solved in two

steps. In the first step, Dr_G / Dt is taken as an unknown and solved. In the next step, the advection equation for r_G is solved. In both steps, the fourth order Runge-Kutta time integration is used.

2.6 Time splitting of pressure equation

As mentioned in the introduction, the response time of a bubble is much shorter than the time scale of flow. This means that Rayleigh-Plesset equation (7) requires much smaller time step than the other hyperbolic-type equations and it makes the simulation time-consuming. For a more efficient computation, two different time steps are adopted here; one for Rayleigh-Plesset equation and another for the rest of the equations.

When separating Eq. (7), the liquid pressure, which is the boundary condition of Eq. (7) must be corrected every time after Equation (7) is solved with the smaller time step. Thus the authors devised the following approach. Equation (15) is now divided into two equations with the idea of time splitting.

$$\frac{1}{c^2}\frac{\partial p}{\partial t} + \quad {}_j f_L u_{Lj} + \quad {}_j f_G u_{Gj} = 0 \qquad (20.1)$$

$$\frac{1}{c^2}\frac{\partial p}{\partial t} = 4\pi r_G^2 n_G \frac{Dr_G}{Dt} \qquad (20.2)$$

Equation (20.1) denotes the pressure change due to the mass transfer and Equation (20.2) denotes the pressure change due to the radius change of the bubble. So the final procedure is

a) Solve the set of Eqs. (1), (11), (15), and (20.1) with the fluid time step (Δt).

b) Solve the set of Eqs. (7), (20.2) and (13) with the bubble time step ($0.1\Delta t$, for example).

c) Solve Eq. (2) with the fluid time step.

This procedure was found to allow larger time step and relieve the stiffness of the system.

3 Results and discussions

3.1 Two-dimensional simulation

NACA0015 Firstly, flows around NACA0015 wing section are calculated. The grid system is shown in Fig. 3. The number of grid points is 161×41 and 101 points on the wing surface. 231×81 grid is also used. The minimum spacing is 10^{-3} which is rather large but chosen because of a stability problem in some cases. The conditions for the computations are tabulated in Table 1.

Table 1 Conditions for NACA0015 wing section.

angle-of-attack	8.0˚
chord length	10cm
initial radius of bubble nucleus	10μm
uniform flow velocity	10m/s
vapor pressure	2.3×10^9Pa
surface tension	7.2×10^{-2}N/m
Reynolds number	3×10^5

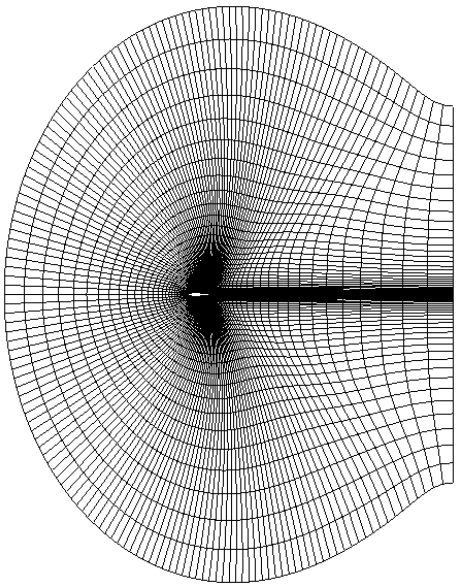

Figure 3: Grid around NACA0015 airfoil.

Each corresponds to the experiment by Kubota et al. (1992). As the Reynolds number is high, the Baldwin-Lomax turbulence model (Baldwin and Lomax 1978) is used to stabilize the boundary layer. At the initial state, the flow is uniform, bubbles are uniformly distributed and have no slip velocities. At the body surface, velocity condition is no-slip or slip wall for both phases, pressure and the number density have no gradient normal to the wall and the bubble radius is zeroth-order-interpolated. For the inflow condition, the pressure gradient is zero and the other variables are fixed at the initial (uniform) condition. For the outflow condition, the pressure is only fixed and other variables are zeroth-order-interpolated. At the permeable surface, all variables are averaged from the upper and the lower points.

Before following the procedure described in 2., a quasi-equilibrium (but not physical) flow field is calculated first. Equation (7) is replaced with,

$$r_G \frac{D^2 r_G}{Dt^2} + \frac{3}{2}\left(\frac{Dr_G}{Dt}\right)^2 = \frac{p_B - p_L}{\rho_L} + \frac{1}{4}\left(u_{Li} - u_{Gi}\right)\left(u_{Li} - u_{Gi}\right) = 0 . \qquad (21)$$

This means that the bubble is in local equilibrium and combined with Eq. (9), Equation (21) directly gives the bubble radius. In this stage, Equation (21) is solved with the same Δt as the other equations. Local time stepping is employed for the convergence acceleration. After obtaining the converged solution, calculation starts with the solution as an initial condition. Physical time stepping with very small time step (order of 10^{-5} of non-dimensional time) is used for the original set of equations toward the steady state. The reason of this procedure is that very large number of time steps would be required to obtain a steady solution with such very small time step and, moreover, bubbles would react with the sudden pressure drop at the initial stage of the computation in lower cavitation number s and might reach unphysical solutions. The number of total time steps for one condition is order of tens to hundreds of thousands and it costs several to tens of hours with a PC of Pentium III 800MHz.

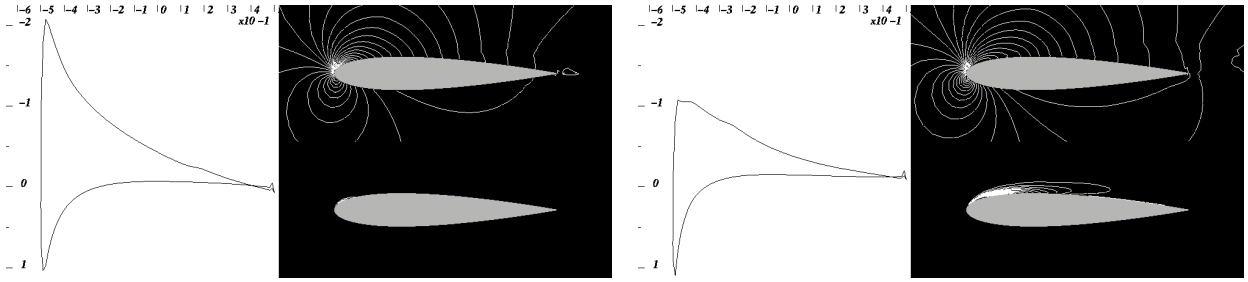

(a) σ=2.0 (b) σ=1.0

Figure 4: Two-dimensional result of flow around NACA0015. Left: Cp distribution. Upper-right: pressure contours. Bottom-right: void fraction contours.

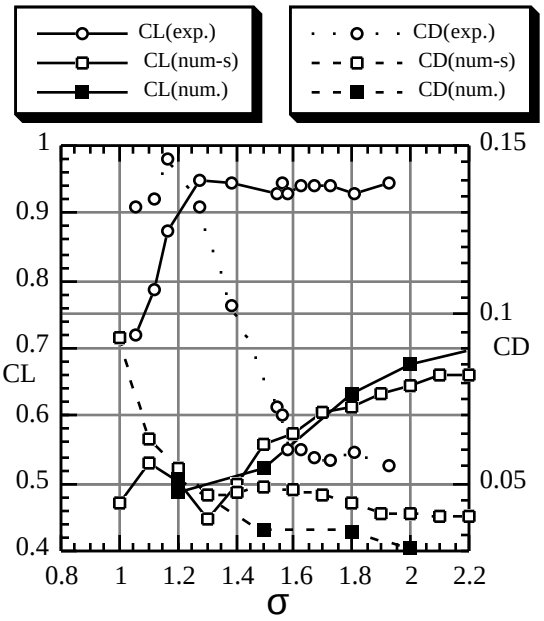

Figure 5: Comparison with experiment of flows around NACA0015 (lift and drag coefficients vs. cavitation number).

Figure 4 shows Cp distribution on the wing, pressure and void fraction contours in the flow field for some cavitation numbers of mostly converged solutions. σ denotes the cavitation number. Solutions fluctuate in time especially in the cases of lower cavitation numbers and results in Fig. 4 are averaged data of last 2000 steps. From the figure, the cavitations occur around the lowest pressure region and are concentrated near the wing surface. The Cp distributions show that the pressure in the cavity is almost the same as the vapor pressure. In the case of lower cavitation number, however, a small spike appears in front of the cavitation region. This is because of the time lag of the bubble response. A comparison with an experiment by Kubota et al. (1992) is shown in Fig. 5. $C_L - \sigma$ and $C_D - \sigma$ curves are plotted. "exp" denotes the experiment, "num-s" the computation with the smaller grid and "num" the computation with the larger grid. Between two grid systems, the differences are relatively small. Compared with the experiments, the tendency agrees but there is still discrepancy in the magnitude.

Walchner Profile 7 and Clark Y-11.7 Another two kinds of wing sections are examined in order to find out the reason of the discrepancy of the previous computation with the experiment. Figure 6 shows the $C_L - \sigma$ plots of the computation and the experiment (Knapp et al. 1970) of Walchner Profile 7 wing section. The grid system is similar to that of NACA0015 but the grid points are 281×41 and 181 points are on the wing surface. The flow conditions are also similar except the angle-of-attack is 0.0˚ and the Reynolds number is 5×10^5. The computation and the experiment agrees better than that in the case of NACA0015. Another is Clark Y-11.7 wing section. Figure 7 shows that comparison of

$C_L - \sigma$ plots (Knapp et al. 1970). The grid size is the same as Walchner Profile 7 and now the angle-of-attack is 2.0˚ and the Reynolds number is 6×10^5. Again the agreement is much better than NACA0015 case.

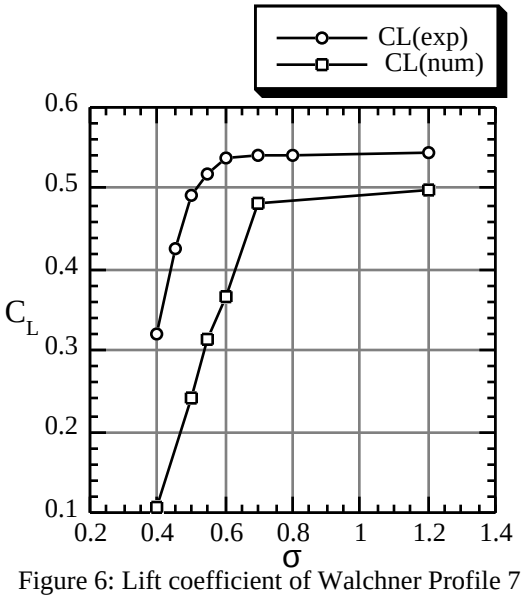

Figure 6: Lift coefficient of Walchner Profile 7

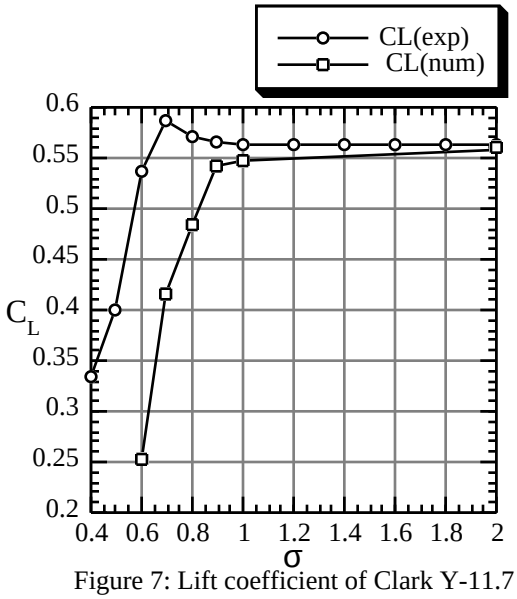

Figure 7: Lift coefficient of Clark Y-11.7

The reason why the level of agreement between the computation and the experiment differ with the airfoil shapes is considered coming from the pressure distribution. In NACA0015 case, the suction peak of the upper surface is very sharp as observed in Fig. 4. Thus the bubble nuclei experience a sudden pressure drop and a sudden pressure recovery. The bubbles on the upper surface expand more than 10 times and soon shrink (or collapses) again. This is physically true for one single bubble. In reality, however, suddenly expanding bubble may interact with other bubbles or form a sheet cavitation or something that the present model dose not include. We believe that the present model is valid for a single bubble but may need another model for bubbles in a sudden pressure change or high void fraction regions.

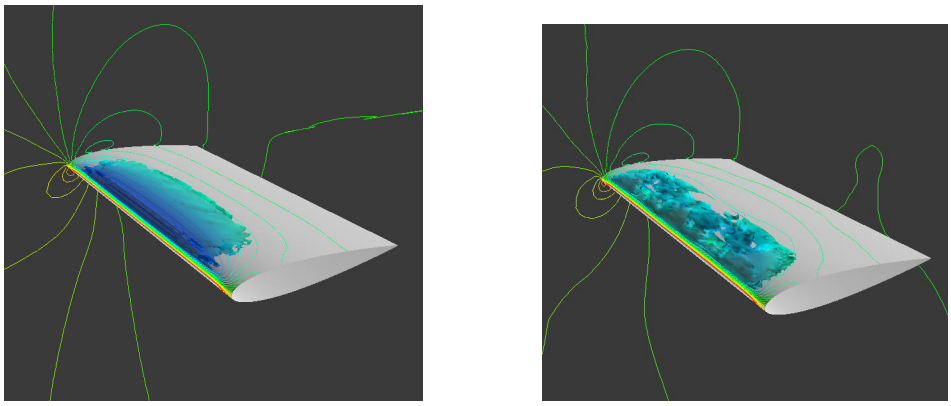

(a) σ=1.5 (b) σ=1.0

Figure 8: Instantaneous flow field (pressure contour and isosurface of void fraction).

3.2 Three-dimensional Simulation

Three-dimensional simulations are preliminary but presented here to demonstrate applicability of the preset method for the three-dimensional problems.

The three-dimensional grid is created by stacking the previously used two-dimensional grid around NACA0015 in the spanwise direction. One boundary of the span direction is a wall and other is the symmetry plane. This simulates a wing of aspect ratio of 2 in a channel. The upper and the lower boundary is considered infinitely far. All the other conditions are the same as the case of the two-dimensional simulations. The number of grid points is $161 \times 32 \times 41$.

Figures 8 (a), (b) show the pressure contour plots on the side wall and iso-void fraction surfaces of the equilibrium solution. The cavitation number is 1.5 and 1.0. Fluctuations of iso-void fraction surface are observed particularly in the case of σ=1.0. In Fig. 9, iso-void fraction surfaces together with the streamlines from the upstream are plotted from two different view angles. The streamlines separate the high void fraction region into two. One is the cavity in the separation and the other the cavity flowing downstream. Even though the result cannot be validated as no experiment corresponds to this condition, the computed flow field is considered consistent to the physics. The CPU time consumed for such time steps is several days with the same PC as the two-dimensional simulations. Larger computer or a parallelization of the code might be necessary for the practical applications.

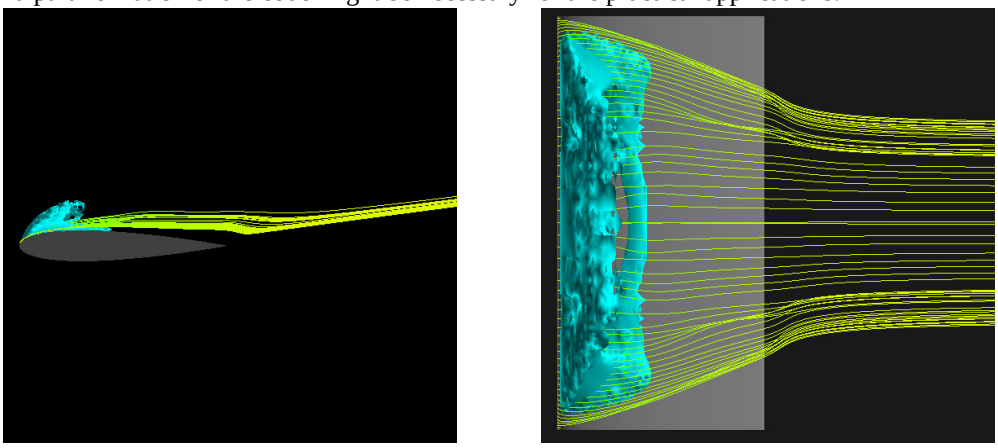

Figure 9: Iso-void fraction surfaces and streamlines (σ=1.0). Left: side view. Right: top view.

4 Conclusions

The dynamics of cavitation bubbles has been modeled and incorporated into the set of governing equations of cavitating flows. The numerical method solving the system of equations were also presented. Two-dimensional simulations showed agreement with the experiments qualitatively. Improvement of the present model is still necessary for the qualitative discussion. Three-dimensional simulations also showed practicality of the present method in efficiency and hope for applications to more practical flow field. More flow fields of both two-dimensional and three-dimensional are to be simulated in the future. Also the application to the rotating flows (in pumps or compressors, for instance) is another future work.

References

BALDWIN, B. S. and LOMAX, H. 1978 Thin Layer Approximation and Algebraic Model for Separated Turbulent Flows. AIAA Paper 78-275.

CHEN, Y. and HEISTER, S. D. 1996 Modeling Hydrodynamic Nonequilibrium in Cavitating Flows. *J. fluid. Eng.*, **118**, 172-178.

DELAUNAY, Y. and KUENY, J. L. 1990 Cavity Flow Predictions Based on the Euler Equations. *ASME Cavitation and Multi-Phase Flow Forum*, **109**, 153-158.

KNAPP, R. T. et al. 1970 *Cavitation. Engineering Societies Monographs*, McGraw-Hill, 267-320.

KUBOTA, A. et al. 1992 A New Modeling of Cavitating Flows. *J. Fluid Mech.*, 240, 59-96.

KUNZ, R. F. et al. 1999 A Preconditioned Navier-Stokes Method for Two-Phase Flows with Application to Cavitation Prediction. AIAA Paper 99-3329.

LEMONNIER, H. and ROWE, A. 1998 Another approach in Modeling Cavitation Flows. *J. Fluid Mech.*, **195**, 557-580.

MATSUMOTO, Y. et al. 1998 Numerical Study of Cavitating Flow Structure on a Hydrofoil. *Proc. 4th KSME-JSME Fluid Eng. Conf.*, 249-252.

MERKLE, C. L. et al. 1998 Computational Modeling of the Dynamics of Sheet Cavitation. *3rd Int. Symp. Cavitation.*

TAKEMURA, F. and MATSUMOTO, Y. 1994 Internal Phenomena in bubble Motion. Bubble Dynamics and Interface Phenomena, KLUWER, 467-474.

VAN LEER, B. 1979 Toward the Ultimate Conservative Difference Scheme. 5, Second -Order Sequel to Godunov's Method. *J. Comp. Phys.*, **32**, 101-136.

YOON, S. and JAMESON, A. 1988 Lower-Upper Symmetric-Gauss-Seidel Method for the Euler and Navier-Stokes Equations. *AIAA J.*, **26**, 1025-1026.